*materials*

MDPI

*Article*

# Improved $NO_x$ Storage/Release Properties of Ceria-Based Lean $NO_x$ Trap Compositions with $MnO_x$ Modification

**Marcos Schöneborn [1,*], Thomas Harmening [1], Javier Giménez-Mañogil [2], Juan Carlos Martínez-Munuera [2] and Avelina García-García [2,*]**

1 SASOL Advanced Materials, Anckelmannsplatz 1, 20537 Hamburg, Germany
2 MCMA Group, Department of Inorganic Chemistry and Institute of Materials, University of Alicante, Carretera Sant Vicent del Raspeig s/n, 03690 Sant Vicent del Raspeig, Alacant, Spain
* Correspondence: marcos.schoeneborn@de.sasol.com (M.S.); a.garcia@ua.es (A.G.-G.); Tel.: +49-40636841241 (M.S.); Tel.: +34-965909419 (A.G.-G.)

Received: 29 May 2019; Accepted: 1 July 2019; Published: 2 July 2019


**Abstract:** Ceria/spinel-based lean $NO_x$ trap compositions with and without barium were modified with $MnO_x$ via incipient wetness impregnation. The effect of the $MnO_x$ layer on the aged materials (850 °C) as to the $NO_x$ storage and release properties was investigated via $NO_x$ adsorption (500 ppm NO/5% $O_2$/balance $N_2$) carried out at 300 °C in a dual-bed with a 1% $Pt/Al_2O_3$ catalyst placed upstream of the samples to generate sufficient amounts of $NO_2$ required for efficient $NO_x$ storage. Subsequent temperature programmed desorption (TPD) experiments were carried out under $N_2$ from 300 °C to 700 °C. The addition of $MnO_x$ to the barium free composition led to a slightly reduced $NO_x$ storage capacity but all of the ad-$NO_x$ species were released from this material at significantly lower temperatures ($\Delta T \approx 100$ °C). The formation of a $MnO_x$ layer between ceria/spinel and barium had a remarkable effect on ageing stability as the formation of $BaAl_2O_4$ was suppressed in favour of $BaMnO_3$. The presence of this phase resulted in an increased $NO_x$ storage capacity and lower desorption temperatures. Furthermore, $NO_x$ adsorption experiments carried out in absence of the Pt-catalyst also revealed an unexpected high $NO_x$ storage ability at low $NO_2$/NO ratios, which could make this composition suitable for various lean $NO_x$ trap catalysts (LNT) related applications.

**Keywords:** ceria; manganese; barium; spinel; lean NOx trap; passive $NO_x$ adsorber; $NO_x$ storage; NO oxidation

## 1. Introduction

The implementation of stricter environmental legislations for passenger cars globally, like Euro 6d, US Tier 3 and China 6B calls for improved catalytic systems for emission control [1]. A lot of attention is drawn to the development of improved $NO_x$ abatement systems ($deNO_x$) for lean-burn engines. As these engines operate at $\lambda > 1$, the abatement of $NO_x$ requires dedicated technologies, such as selective catalytic reduction (SCR) and lean $NO_x$ trap catalysts (LNT), also known as $NO_x$ storage/reduction catalysts (NSR) [2,3].

In SCR systems, an aqueous urea solution is injected into the exhaust gas via an onboard-tank leading to the formation of $NH_3$, which then reacts with $NO_x$ over the catalyst via the standard (1) and fast (2) SCR reactions. Currently, the most common SCR catalysts are metal-substituted zeolites, like Fe-ZSM-5 or Cu-CHA [4].

$$4NO + 4NH_3 + O_2 \rightarrow 4N_2 + 6H_2O \quad (1)$$

$$NO + NO_2 + 2NH_3 \rightarrow 2N_2 + 3H_2O \quad (2)$$

The fast SCR reaction (2) is significantly more effective than reaction (1) at low temperatures in the range of 250–300 °C but it requires the presence of $NO_2$. Therefore, the SCR catalyst is typically positioned downstream of the diesel oxidation catalyst (DOC), which effectively increases the $NO_2/NO_x$ ratio [5,6]. Once the $NO_2$ concentration exceeds a certain threshold, the $NO_2$-SCR reaction (3) also takes place.

$$4NH_3 + 3NO_2 \rightarrow 7/2N_2 + 6H_2O \quad (3)$$

The $NO_x$ abatement mechanism of lean $NO_x$ traps is based on alternating lean/rich cycles with long lean phases, in which $NO_x$ emissions from the exhaust gases are adsorbed on the catalyst. The stored ad-$NO_x$ species are desorbed and reduced to nitrogen on catalytically active noble metals in subsequent short rich periods at elevated temperatures [7]. Most common lean $NO_x$ trap catalysts contain a high surface-area material like $\gamma$-$Al_2O_3$, mixtures of BaO and $CeO_2$ and noble metals, typically Pt or Pd and Rh [8,9].

Barium species, such as BaO or $BaCO_3$ act as the primary $NO_x$ storage component. They can adsorb large amounts of $NO_x$ in the form of surface nitrites and nitrates during lean operation which involves the progressive oxidation from NO to $NO_2$ and finally $NO_3^-$. The mechanism of $NO_x$ adsorption on barium species has been investigated intensively [10–15]. According to these studies, the $NO_x$ adsorption takes place via two pathways in parallel. In the "nitrite" route, NO is catalytically oxidized and directly stored on barium sites in form of nitrite ad-species which can be further oxidized to nitrates.

The "nitrate" route is initiated by the catalytic oxidation of NO to $NO_2$ (4) which then react on barium sites in a disproportionation reaction, resulting in the formation of nitrate and NO (5).

$$NO + 1/2O_2 \rightarrow NO_2 \quad (4)$$

$$3NO_2 + BaO \rightarrow Ba(NO_3)_2 + NO \quad (5)$$

The regeneration of $NO_x$ storage sites occurs during rich periods and forms harmless nitrogen via the reduction of $NO_x$ species with hydrogen. Cumaranatunge et al. proposed a mechanism that involves the intermediate generation of ammonia [16]. This mechanism has been confirmed in following studies in which various analytical techniques were applied [17,18]. The fundamental chemical reactions can be summarized as:

$$Ba(NO_3)_2 + 8H_2 \rightarrow 2NH_3 + BaO + 5H_2O \quad (6)$$

$$3Ba(NO_3)_2 + 10NH_3 \rightarrow 8N_2 + 3BaO + 15H_2O \quad (7)$$

The addition of ceria, which has become a major component in catalyst compositions leads to superior $NO_x$ storage efficiencies, especially at temperatures below 300 °C [19,20]. Furthermore, ceria plays a substantial role in the water-gas-shift reaction as it provides hydrogen for the regeneration during rich periods and it has a positive impact on the $NO_x$ storage/release chemistry due to its interplay with platinum [21–24]. The mechanisms of $NO_x$ storage on ceria under lean conditions involve the formation of various ad-$NO_x$ species, such as linear, bidentate and chelating nitrites and nitrates. It was observed that the low-temperature (<100 °C) adsorption of NO on ceria primarily leads to the generation of surface nitrites whereas at higher temperatures nitrates are preferentially formed [19,25,26]. On the contrary, Ryou et al. did not observe the formation of nitrates on $Pd/CeO_2$ at 120 °C and they proposed that the presence of water suppresses the oxidation of nitrites [27]. The adsorption of $NO_2$ on ceria was studied in detail by Flitschew et al. who combined the well-established diffuse reflectance infrared Fourier transform spectroscopy (DRIFTS) with *in-situ* Raman spectroscopy [28,29]. The authors elaborated that $NO_2$ storage on ceria proceeds mainly in two pathways which both lead to the formation nitrate species. The first route involves the adsorption of $NO_2$ on cerium(III) sites which are thereby oxidized and transformed to active Ce(IV)-O species (8) which can then react with additional $NO_2$ to form nitrates (9). In the second pathway, $NO_2$ reacts directly with Ce(IV)-O sites without the contribution of cerium(III) (9).

$$Ce(III) + NO_2 \rightarrow Ce(IV) \cdots O^{2-} + NO \quad (8)$$

$$Ce(IV) \cdots O^{2-} + NO_2 \rightarrow Ce(III) \cdots O\text{-}NO_2^{-} \quad (9)$$

Fine-tuning of the regeneration parameters, like temperature and modes of fuel-injection is a demanding task and crucial for the performance such as the long-time durability of the catalyst. Incomplete regeneration inevitably leads to catalyst degradation over time as relevant surface sites remain occupied with adsorbed $NO_x$ species. On the contrary, excess $H_2$ formed during long rich cycles and low temperatures leads to the generation of high levels of ammonia. This can be a serious concern in LNT-only systems [18,30]. Another important aspect to be considered is the additional fuel-consumption required to enrich the exhaust gas, which eventually leads to increased $CO_2$ emissions. Therefore, $NO_x$ storage compounds that can effectively be regenerated are urgently needed.

The synergetic combination of passive SCR with LNT catalysts is an efficient solution to attain low $NO_x$ tailpipe emissions and to cope with high levels of $NH_3$, which may result from the total reduction of $NO_x$. This approach has become a widespread and well-studied technology for several years [31–38]. The low-temperature performance of LNT complements SCR and the ammonia generated during the rich regeneration phase can replace or supplement urea required for the SCR reactions.

One major deactivation mechanism of LNT catalysts is the solid acid-base reaction between $Al_2O_3$ and BaO at elevated temperatures resulting in the formation of $BaAl_2O_4$ and thus causing a loss of $NO_x$ adsorption sites [39,40]. Improvements in this regard have been reported via the replacement of alumina with the less acidic spinel ($MgAl_2O_4$), leading to the formation of $BaAl_2O_4$ only at higher temperatures [41,42]. In addition, the use of spinel in LNT catalysts has been described to improve the low temperature $NO_x$ storage efficiency and to contribute to enhanced $SO_x$ tolerance via the formation of sulphates with low thermal stability [43].

Another reported deactivation mechanism results from reaction of BaO and $CeO_2$ yielding $BaCeO_3$, which was detected in LNT formulations prepared by the impregnation of ceria with barium salts [44].

Despite the technological and chemical improvements achieved over the past 20 years, deactivation at elevated temperatures and optimized $NO_x$ storage/release properties are perpetual challenges in the design of new formulations for LNT catalysts.

In this regard, the addition of manganese to LNT compositions aiming at improved performance has been proposed and studied by several authors. $MnO_x$ –$CeO_2$ mixed oxides present high oxygen storage abilities and improved redox properties. They are typically obtained by coprecipitation, sol-gel synthesis or similar routes leading to highs level of homogeneity. The interesting properties predestine these mixed oxides for a substitution of pure ceria in various applications and their superior ability to oxidize soot and NO has already been reported [45–47]. Le Phuc et al. observed significantly improved performance of $MnO_x$-$CeO_2$ containing Pt/Mn-Ce/Ba/Al LNT catalysts in $NO_x$ reduction during rich phases, which they attributed to the improved oxygen mobility of the mixed oxide as compared to pure $CeO_2$ [48].

In another work, Le Phuc studied the contribution of crystalline $Mn_2O_3$ as to the $NO_x$ storage performance in Mn/Ba/Al compositions which were investigated in the fresh state, that is, without applying thermal ageing prior to testing [49]. It was found that the manganese sesquioxide only led to improved $NO_x$ storage performance in a narrow compositional range whereas higher or lower concentrations had a detrimental effect on the storage efficiency.

Zhang et al. detected the formation of $BaMnO_3$ in the system Pd/Mn/Ba/Al. The presence of this phase led to superior NO oxidation abilities and $NO_x$ storage performances of the fresh catalysts [50]. Similar but not identical observations were made by Xiao et al, who noticed the occurrence of $BaMnO_3$ only after calcination at 800 °C [51]. This is in accordance with our own investigations, in which we detected this phase in the system Al/Mg/Ce/Mn/Ba after calcination at 850 °C [52].

However, the impact of ageing at elevated temperature as to the $NO_x$ storage/release properties of the manganese modified formulations has not been reported yet.

In this work, we present a novel route for the preparation of manganese modified LNT compositions leading to a $MnO_x$ layer on ceria/spinel mixtures rather than homogeneous $MnO_x$-$CeO_2$ mixed oxides. Firstly, the impact on this route in altering the $NO_x$ storage/release properties of the resulting spinel/ceria/manganese compositions is investigated. Secondly, the stabilizing function of the $MnO_x$ layer as a protective barrier between spinel/ceria and barium is rationalized. The materials described herein were thermally aged at 850 °C prior to testing in order to study their thermal stability, which is a common procedure to simulate catalyst ageing under real conditions [53]. $NO_x$ storage experiments were carried in a dual-bed with a 1% $Pt/Al_2O_3$ catalyst placed upstream from the samples. This arrangement mimics a diesel oxidation catalyst, which is typically present in state-of-the-art lean-burn catalyst systems and generates high concentrations of $NO_2$. It was shown in previous studies that $NO_2$ can be stored much more efficiently than NO on barium and cerium species [19,54].

In order to study the NO oxidation ability provided by the manganese species, additional $NO_x$ adsorption experiments were carried out in absence of the Pt/alumina catalyst.

The thermal stability of the ad-$NO_x$ species is important to estimate how efficiently the corresponding $NO_x$ storage sites can be regenerated. Therefore, the $NO_x$ release properties of our new formulations were investigated in temperature programmed desorption (TPD) experiments.

## 2. Materials and Methods

### 2.1. Sample Preparation

$MnO_x$ modified carriers with loadings of 9 wt% (calculated as $MnO_2$) were prepared by incipient wetness impregnation of homogeneous compositions $MgAl_2O_4/CeO_2$ (PURALOX MG20 Ce20, commercially available from SASOL) using an aqueous solution of manganese acetate tetrahydrate. The dried samples were then calcined in air at 600 °C.

Both, the Mn-free and the Mn-modified materials were used as starting materials for further wet-impregnation with a barium acetate solution to obtain a loading of approximately 15 wt% BaO. All samples were aged in air at 850 °C for 4 h prior to analyses. Henceforth, the samples are referred to as MgCe (PURALOX MG20 Ce20), MgCe-Mn (MgCe modified with $MnO_x$), MgCe-Ba (MgCe modified with BaO) and MgCe-Mn-Ba (MgCe subsequently modified with $MnO_x$ and BaO). The chemical compositions of the samples are summarized in Table 1.

**Table 1.** Chemical composition (wt%) of the samples determined by Inductively Coupled Plasma (ICP) analysis.

| Sample | $Al_2O_3$ | MgO | $CeO_2$ | $MnO_2$ | BaO |
|---|---|---|---|---|---|
| MgCe | 63.0 | 17.0 | 20.0 | 0 | 0 |
| MgCe-Mn | 58.3 | 14.9 | 17.7 | 9.1 | 0 |
| MgCe-Ba | 52.8 | 14.7 | 17.0 | 0 | 15.5 |
| MgCe-Mn-Ba | 48.4 | 13.3 | 15.5 | 7.3 | 15.5 |

### 2.2. Sample Characterization

Surface area (Brunauer-Emmett-Teller method, BET) and porosity measurements were performed by nitrogen adsorption at −196 °C using a Micromeritics Tri-Star 3000 system. The samples were outgassed overnight at 300 °C under vacuum prior to the measurements. X-ray powder diffraction was conducted on a Phillips X'Pert diffractometer using Cu-Kα radiation (λ = 1.540598 Å). Powder diffractograms were recorded between 5° and 90° (2θ), with a step-width of 0.02°. The sample compositions were determined after digestion in an MLS 1200 microwave apparatus by Inductively Coupled Plasma Atomic Emissions Spectrometer (ICP-OES) using a Spectroflame instrument (SPECTRO). X-ray photoelectron spectra (XPS) were obtained using a K-alpha spectrophotometer (Thermo-Scientific), with a high-resolution monochromator. It comprises a source of electrons and ions for automated load compensation. The X-ray radiation source is equipped with an Al anode (1486.6 eV). The pressure of the analysis chamber was constantly set at $5 \times 10^{-9}$ mbar. The detector

was kept in constant energy mode with a pass energy of 200 eV for the survey spectrum and 50 eV for the sweep in each individual region. The binding energy was adjusted using the C-1s transition, appearing at 284.6 eV. Binding energy values measured are accurate to ±0.2 eV. The values of binding energy and kinetic energy were adjusted with the Peak-Fit software of the spectrophotometer. The Mg-1s, Al-2p, Ce-3d, Mn-2p, Ba-3d regions (along with C-1s and O-1s regions) were employed to analyse the surface composition of the carriers in the present study.

### 2.3. $NO_x$ Storage/Release Tests

$NO_x$ adsorption experiments were conducted in a quartz tubular reactor connected to specific NDIR-UV gas analysers for NO, $NO_2$, CO, $CO_2$ and $O_2$, with the measurement data recorded every 10 seconds. The $NO_x$ adsorption (500ppm NO/5%$O_2$/balance $N_2$) was performed at 300 °C in a dual-bed configuration with a 1% Pt/$Al_2O_3$ commercial catalyst (supplied by Sigma-Aldrich) placed upstream of the sample using a global flow gas of 500 mL/min. The catalyst effectively oxidizes NO to $NO_2$, which is required for effective $NO_x$ storage. Subsequent temperature programmed desorption (TPD) experiments were carried out under $N_2$ from 300 °C to 700 °C (5 °C/min) in order to study the thermal stability of the various stored $NO_x$ species. Besides $NO_x$ storage ability, this is another important aspect in order to assess the suitability of the different materials for the development of new LNT catalysts.

In addition, $NO_x$ adsorption experiments in single-bed configuration were performed without the Pt/alumina catalyst in order to study the NO oxidation ability of the individual samples and to gain further insight into the role of the individual manganese species in the $NO_x$ storage processes.

## 3. Results

### 3.1. Structural Properties

The phase composition of the samples was analysed by powder X-ray diffraction. It can be seen in Figure 1 that all samples contain $MgAl_2O_4$ and $CeO_2$ in crystalline form.

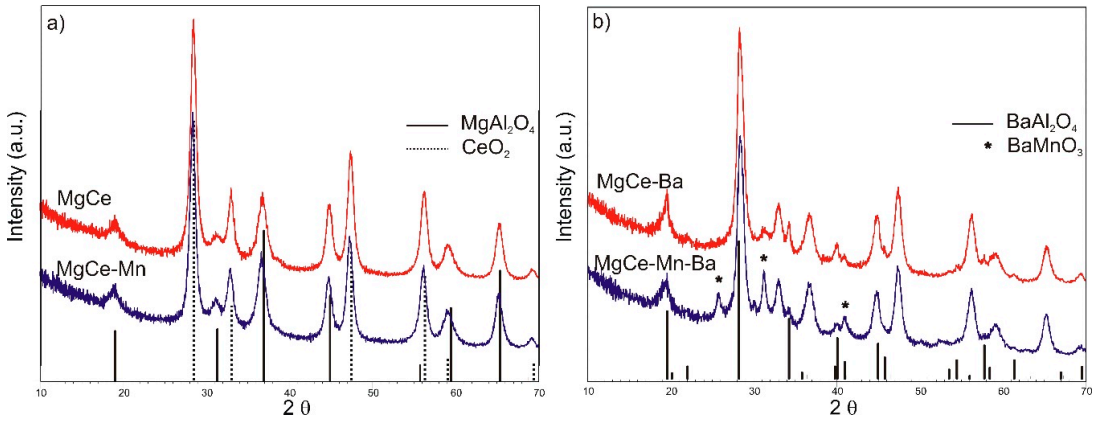


**Figure 1.** Powder X-ray diffraction (XRD) patterns of (**a**) MgCe and MgCe-Mn (**b**) MgCe-Ba and MgCe-Mn-Ba with simulated reflection positions of $MgAl_2O_4$, $CeO_2$, $BaAl_2O_4$ and $BaMnO_3$. For better clarity, the reflections of $MgAl_2O_4$ and $CeO_2$ are not marked in (**b**).

The addition of $MnO_x$ to the $MgAl_2O_4$/$CeO_2$ composition does not lead to the occurrence of additional reflections in the powder pattern, thus pointing to a homogeneous dispersion of the $MnO_x$ species among the surface without the formation of additional crystalline domains detectable by X-ray diffraction (XRD).

The Ba-containing samples with and without manganese exhibit remarkable differences. In MgCe-Ba, a substantial formation of crystalline $BaAl_2O_4$ is observed. This phase is also present in MgCe-Mn-Ba but the intensity of the relevant reflections is decreased in the X-ray pattern of this material. Most importantly, the formation of $BaMnO_3$ is detected in MgCe-Mn-Ba. This phase

adopting the perovskite structure is more accurately described as $BaMnO_{3-\delta}$, reflecting the possible formation of vacancies in the oxygen sublattice in conjunction with a partial reduction of manganese (IV). The presence of this phase indicates a close proximity of barium and manganese achieved via the preparation procedure and is in accordance with previous studies, in which the occurrence of $BaMnO_3$ in the systems $Ba/MnO_x$-$CeO_2$ and $Mn/Ba/Al_2O_3$ was also reported [48,50,51,55,56]. No indication of crystalline binary manganese oxides is found in the XRD pattern of MgCe-Mn-Ba. Other authors, however, reported on the occurrence of isolated and crystalline species $Mn_2O_3$ or $MnO_2$ in similar systems [49,50]. Remarkable structural and compositional differences of manganese modified supports as a function of the use of either Mn-acetate or Mn-nitrate for preparation were observed and studied by Kapteijn et al., underlining the crucial role of the preparation route as to the resulting phase composition and arrangement [57]. No indication of the presence of $BaCeO_3$ is found in either sample, proving that the formation of this phase is thermodynamically unfavoured under the conditions of preparation and ageing.

Data on the physical properties of all samples is summarized in Table 2.

**Table 2.** Physical properties of the samples studied in this work.

| Sample | $S_{BET}$ ($m^2$/g) | $r_P$ (nm) | $V_P$ ($cm^3$/g) |
|---|---|---|---|
| MgCe | 96 | 13 | 0.64 |
| MgCe-Mn | 104 | 10 | 0.53 |
| MgCe-Ba | 68 | 11 | 0.37 |
| MgCe-Mn-Ba | 59 | 11 | 0.31 |

Incorporation of about 15% of BaO on the solid precursors by means of wet impregnation followed by aging at 850 °C leads to a significant decrease in BET surface areas and pore volumes of the resulting samples. Nevertheless, the large average pore radius present in all samples is a good indication of their suitability as functional supports for LNT catalysts.

The analysis of the XPS results (Table 3) becomes complex because the samples suffer from significant levels of carbon contamination due to the presence of carbonates. Carbonation also inevitably occurs under real exhaust conditions. Therefore, purging of the samples via heat treatment in inert gas prior to the $NO_x$ storage tests was not applied. Considering the sequential preparation of the samples, both the atomic surface analysis and the metal ratios broadly reflect the decrease in Al, Mg and Ce content after addition of manganese and barium. In addition, the decrease in manganese content after subsequent impregnation with barium is reflected by the XPS results.

**Table 3.** Surface atomic contents and ratios estimated by X-ray photoelectron spectroscopy (XPS).

| Element | Sample | | | |
|---|---|---|---|---|
| | MgCe | MgCe-Mn | MgCe-Ba | MgCe-Mn-Ba |
| C | 33.46 | 43.7 | 50.4 | 58.1 |
| O | 40.0 | 37.7 | 35.5 | 30.1 |
| N | 0.4 | 0.3 | 0.7 | 0.5 |
| Al | 17.3 | 11.1 | 10.5 | 8.5 |
| Ce | 2.9 | 2.5 | 0.7 | 0.5 |
| Mg | 2.3 | 2.3 | 1.1 | 1.0 |
| Mn | 0.0 | 2.5 | 0.0 | 0.7 |
| Ba | 0.0 | 0.0 | 1.2 | 0.8 |
| Al/(Al + Ce + Mg + Mn + Ba) [1] | 0.77 | 0.60 | 0.78 | 0.74 |
| Ce/(Al + Ce + Mg + Mn + Ba) [1] | 0.13 | 0.14 | 0.05 | 0.04 |
| Mg/(Al + Ce + Mg + Mn + Ba) [1] | 0.10 | 0.13 | 0.08 | 0.09 |
| Mn/(Al + Ce + Mg + Mn + Ba) [1] | - | 0.13 | - | 0.06 |
| Ba/(Al + Ce + Mg + Mn + Ba) [1] | - | - | 0.09 | 0.07 |

[1] The ratios were calculated based on the content of the elements.

### 3.2. $NO_x$ Storage

#### 3.2.1. Dual-bed Experiments

The results of the $NO_x$ adsorption tests measured in dual-bed configuration are displayed in Table 4.

**Table 4.** Amounts of $NO_x$ stored on the samples in dual-bed experiments.

| Samples without Ba | $NO_x$ Stored ($10^{-3}$ mmol/$m^2_{carrier}$) | Samples with Ba | $NO_x$ Stored ($10^{-3}$ mmol/$m^2_{carrier}$) |
|---|---|---|---|
| MgCe | 3.23 | MgCe-Ba | 4.41 |
| MgCe-Mn | 2.60 | MgCe-Mn-Ba | 6.27 |

The total $NO_x$ retention capacity expressed as mmol of $NO_x$ stored/$m^2$ of carrier follows the order—MgCe-Mn < MgCe < MgCe-Ba << MgCe-Mn-Ba. It is worth mentioning that the surface areas of the samples with barium are significantly lower, resulting in a different order of $NO_x$ retention capacity if expressed as mmol of $NO_x$ stored/g of carrier—MgCe-Mn < MgCe-Ba < MgCe << MgCe-Mn-Ba. This is of importance as the reduction in surface area upon Ba-addition and ageing clearly contribute to the deactivation of the support in terms of $NO_x$ storage ability. In order to study the role of the different species present in the samples, the surface area related expression is applied in this work.

In the case of the Ba-free samples, the presence of $MnO_x$ slightly reduces the $NO_x$ storage capacity, thus illustrating that the $MnO_x$ as such does not contribute to the $NO_x$ storage process at all or only to a negligible extend. Apparently, relevant $NO_x$ storage sites of ceria and spinel are partially occupied and thus inactivated by Mn-species. This can also be deduced from the XPS analyses revealing a lower surface concentration of cerium and also a higher surface concentration of carbon species in the $MnO_x$ modified samples. MgCe-Ba (less cerium and magnesium but barium on the surface) shows a marked but unexpected small increase in $NO_x$ retention capacity compared to MgCe, which indicates that only a small amount of unreacted (and X-ray invisible) BaO or $BaCO_3$ is still present after ageing. MgCe-Mn-Ba on the contrary, exhibits superior $NO_x$ storage ability, pointing to a significant stabilizing and hence beneficial effect of $MnO_x$ on the Ba-assisted $NO_x$ storage process. The introduction of $MnO_x$ as protective layer between BaO and spinel/ceria leads to the formation of $BaMnO_3$ and reduces the amount of undesired $BaAl_2O_4$ generated after ageing, as observed in the XRD pattern. Thus, the occurrence of the perovskite phase most likely accounts for the high retained $NO_x$ storage ability after ageing.

#### 3.2.2. Single-bed Experiments

Single-bed experiments without the Pt/alumina catalyst were conducted to study the effect of Mn-addition on NO oxidation ability. The absence of the noble metal catalyst is required as its outstanding oxidation capacity does not allow for a proper investigation of the NO oxidation contribution of the carriers. Table 5 compiles the NO and $NO_2$ levels quantified for the samples MgCe and MgCe-Mn during $NO_x$ adsorption in single-bed experiments. The adsorption curves obtained for MgCe and MgCe-Mn observed in single-bed (SB) and dual-bed (DB) experiments are shown in Figure 2).

**Table 5.** $NO_2$/NO ratios and amounts of $NO_x$ stored on the different samples obtained under single-bed configuration.

| Sample | $NO_2$/NO Ratio | $NO_x$ Stored ($10^{-3}$ mmol/$m^2_{carrier}$) |
|---|---|---|
| MgCe | 0.07 | 1.27 |
| MgCe-Mn | 0.43 | 1.03 |
| MgCe-Ba | 0.08 | 1.40 |
| MgCe-Mn-Ba | 0.48 | 6.39 |

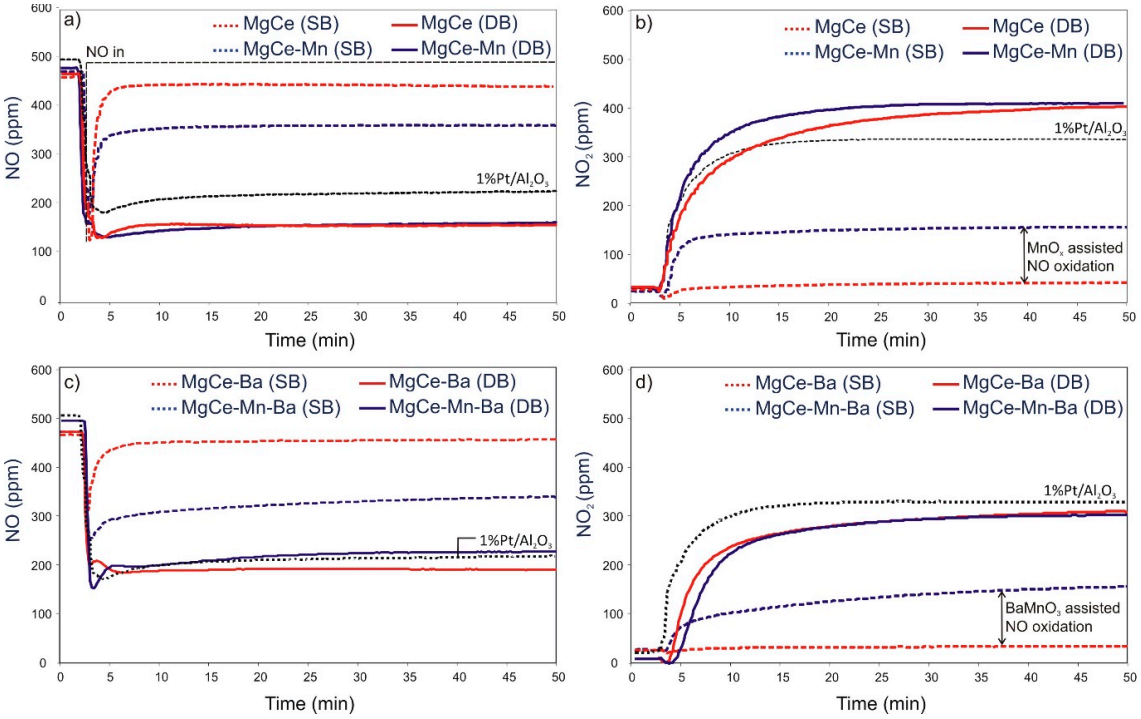


**Figure 2.** Profiles of NO and $NO_2$ of during $NO_x$ adsorption at 300 °C under single-bed (SB) and dual-bed (DB) conditions. (**a**) NO and (**b**) $NO_2$ profiles of MgCe and MgCe-Mn. (**c**) NO and (**d**) $NO_2$ profiles of MgCe-Ba and MgCe-Mn-Ba. Profiles of Pt/alumina are included for comparison.

MgCe-Mn presents a significantly higher $NO_2$ production than MgCe evident from the $NO_2$/NO ratios obtained in single-bed experiments, revealing its superior NO oxidation activity promoted by $MnO_x$ addition. The ability of binary manganese oxides, especially $Mn_2O_3$, to oxidize NO has also been observed and described in detail by Guo et al. [58]. Although the analysis of the oxidation state of manganese is not part of this study, the presence of highly dispersed $Mn_2O_3$ species in MgCe-Mn therefore appears to be a valid assumption.

Although the difference in $NO_2$/NO ratios between MgCe-Ba and MgCe-Mn-Ba is in the same range as in the Ba-free samples, a remarkable higher $NO_x$ storage ability is found in MgCe-Ba-Mn in the single-bed experiments. The amount of stored $NO_x$ is in the same range as observed in dual-bed experiments and is around 4.5 times higher than that observed for MgCe-Ba. The amounts of stored $NO_x$ observed in single-bed and dual-bed experiments are summarized in Figure 3. The NO and $NO_2$ adsorption progressions shown in Figure 2c,d prove that the high $NO_x$ storage efficiency of MgCe-Mn-Ba results from the effective $NO_2$ production in conjunction with the availability of storage sites. NO as such is only adsorbed to a negligible extend. The value of Ba-Mn interactions for fast $NO_x$ storage has previously been reported by Zhang et al. [50]. They have found that the NO oxidation ability of Mn-sites in close proximity to $NO_x$ storage sites of barium leads to very high $NO_x$ storage efficiencies. It can be speculated that the perovskite $BaMnO_3$, which accommodates manganese in the rather high oxidation state +IV, combines both, high redox potential and efficient $NO_x$ storage sites in one solid. The high activity of $BaMnO_3$ for NO and soot oxidation has also been pointed out by Gao et al. [55].

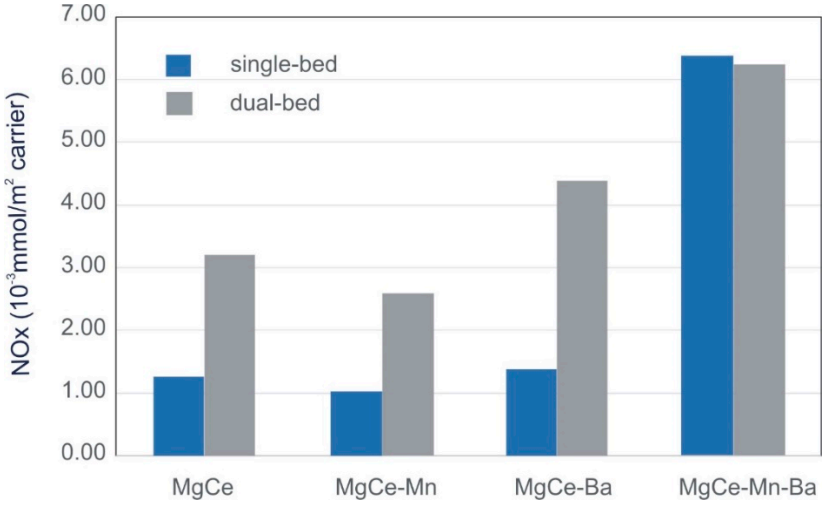


**Figure 3.** Stored amounts of $NO_x$ observed in single-bed and dual-bed experiments.

### *3.3. NOx Release*

#### 3.3.1. TPD after $NO_x$ Adsorption under Dual-bed Configuration

The temperature programmed desorption (TPD) of $NO_x$, NO and $NO_2$ after $NO/O_2$ retention under dual-bed configuration was analysed in the temperature range of 300–700 °C. Figure 4 shows the TPD profiles of the different samples. The shape of the TPD profile of MgCe with two maxima—the first one centred at about 360 °C and the second centred at about 450 °C—indicates that there are two main ad-$NO_x$ species present on this sample. The individual contribution of NO and $NO_2$ with the quantification given in Table 6 reveals that a significant fraction of the stored $NO_x$ is released from this sample in the form of $NO_2$. The $NO_2$ desorption takes places in a wide temperature window between 300 and 510 °C. The release of NO takes place in two steps, the first centred at about 350 °C and the second centred at about 490 °C.

The presence of barium leads to distinct changes in the TPD profiles in MgCe-Ba and MgCe-Mn-Ba. Significantly more NO is released from MgCe-Ba than from MgCe with the concentration of $NO_2$ being almost identical. Similar to MgCe, the NO profile of MgCe-Ba shows two peaks. The first one is centred at about 350 °C and shows a comparative shape and peak area than the corresponding peak in MgCe. The second peak is centred at about 530 °C, with a much larger peak area. The NO release is taking place between 440 °C and 610 °C, so that the maximum desorption temperature of NO is increased by about 120 °C compared to MgCe. The concentrations and release temperatures of $NO_2$ are very similar for MgCe and MgCe-Ba although the main contribution of $NO_2$ in MgCe-Ba originates from the desorption processes taking place between 400 °C and 520 °C.

**Table 6.** Released amounts of $NO_x$, NO and $NO_2$ after adsorption under dual-bed configuration.

| Sample | $NO_x$ Released ($10^{-3}$ mmol/m$^2_{carrier}$) | NO Released ($10^{-3}$ mmol/m$^2_{carrier}$) | $NO_2$ Released ($10^{-3}$ mmol/m$^2_{carrier}$) |
|---|---|---|---|
| MgCe | 2.47 | 0.79 | 1.68 |
| MgCe-Mn | 0.97 | 0.78 | 0.19 |
| MgCe-Ba | 4.69 | 3.15 | 1.54 |
| MgCe-Mn-Ba | 4.76 | 4.39 | 0.37 |

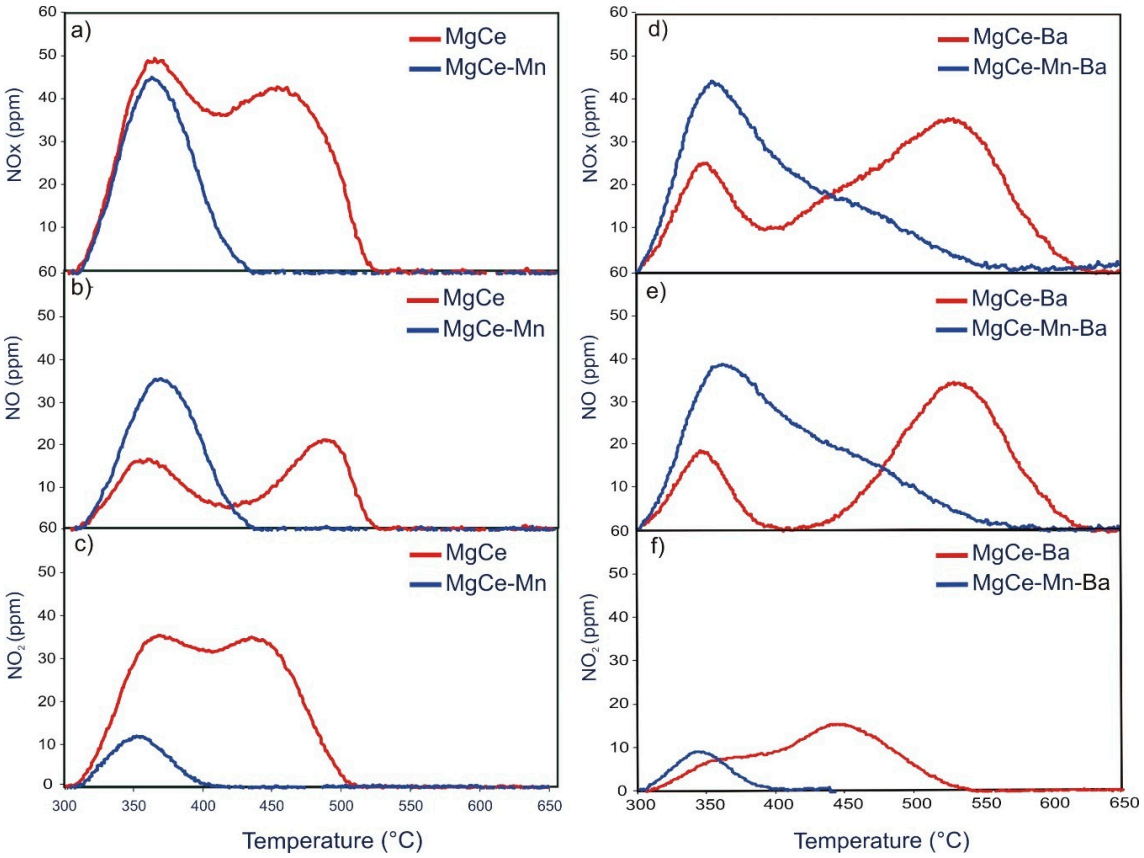


**Figure 4.** Temperature programmed desorption (TPD) profiles (dual-bed configuration) of MgCe and MgCe-Mn (**a**) $NO_x$, (**b**) NO (**c**) $NO_2$ and MgCe-Ba and MgCe-Mn-Ba (**d**) $NO_x$, (**e**) NO (**f**) $NO_2$.

The observations made in the TPD profiles of MgCe and MgCe-Ba lead to the conclusion that the active barium species form comparatively strongly bound ad-$NO_x$ species, which mainly form NO upon decomposition. This is in line with studies from Lietti et al. [11,12], who reported that NO is the main decomposition product of $NO_x$ species stored on barium, with TPD profiles very similar to the high temperature peak shown in Figure 4e. This furthermore supports the assumption (see Section 3.2.1) that there are still active barium species left on MgCe-Ba although only $BaAl_2O_4$ can be detected in the X-ray pattern.

The presence of $MnO_x$ forming a layer on spinel/ceria displays unexpected substantial effects on the $NO_x$ release chemistry of the samples with and without BaO. The $NO_x$ desorption is dominated by NO in the Mn-containing samples with only minor contribution of $NO_2$ in marked contrast to the Mn-free samples. In the case of the Mn-Ba combination, an additional contribution of NO species released in the range of 420–520 °C is observed, thus pointing to the generation of additional storage sites. This contribution can be linked to the presence of $BaMnO_3$ since this desorption peak is absent in MgCe-Mn. Secondly, the $NO_x$ release process is much more efficient in the $MnO_x$ modified samples, in particular in MgCe-Mn. As it can be seen in Figure 4a–c, the $NO_x$ desorption is taking place in the narrow range 300–450 °C. The high temperature desorption of NO and $NO_2$ is completely absent in the $MnO_x$ modified sample. A similar observation is made in the TPD profile of MgCe-Mn-Ba, in which the decreased fraction of $NO_x$ desorbed at higher temperatures upon manganese modification is also apparent.

### 3.3.2. TPD after $NO_x$ Adsorption under Single-bed Configuration

Effects induced by $MnO_x$ addition are even more pronounced in the TPD profiles of MgCe and MgCe-Mn after $NO_x$ storage under single-bed configuration (Figure 5 and Table 7).

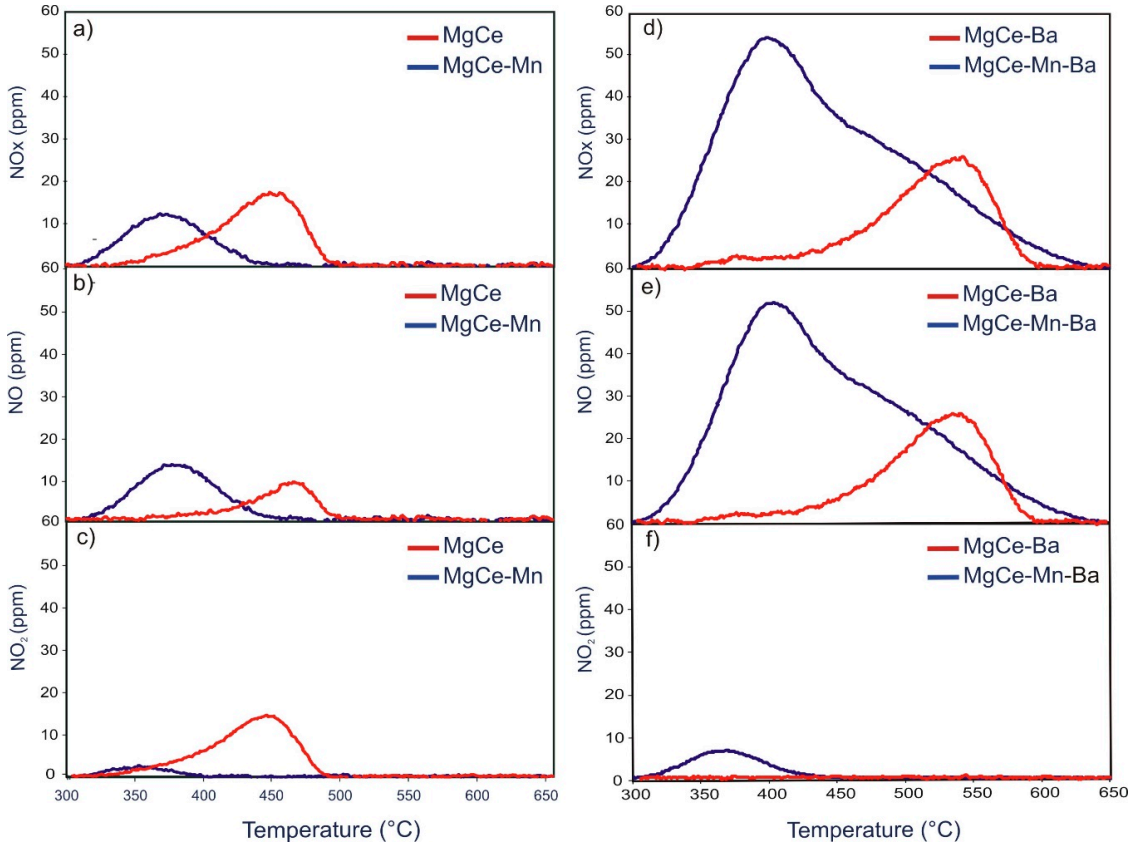


**Figure 5.** TPD profiles (single-bed configuration) of MgCe and MgCe-Mn (**a**) $NO_x$, (**b**) NO (**c**) $NO_2$ and MgCe-Ba and MgCe-Mn-Ba (**d**) $NO_x$, (**e**) NO (**f**) $NO_2$.

**Table 7.** Released amounts of $NO_x$, NO and $NO_2$ after adsorption under single-bed configuration.

| Sample | $NO_x$ Released ($10^{-3}$ mmol/$m^2_{carrier}$) | NO Released ($10^{-3}$ mmol/$m^2_{carrier}$) | $NO_2$ Released ($10^{-3}$ mmol/$m^2_{carrier}$) |
|---|---|---|---|
| MgCe | 0.59 | 0.18 | 0.41 |
| MgCe-Mn | 0.36 | 0.32 | 0.04 |
| MgCe-Ba | 1.34 | 1.34 | 0 |
| MgCe-Mn-Ba | 5.05 | 4.61 | 0.44 |

The majority of stored $NO_x$ species is released from MgCe in the range of about 320–490 °C in the form of $NO_2$. The asymmetry of the $NO_2$ peak indicates the presence of differently bound ad-$NO_x$ species with the main population being desorbed at the peak maximum of about 440 °C.

TPD profiles of MgCe-Mn show a significant increase in NO desorption whereas the concentration of released $NO_2$ is close to zero. The high-temperature desorption peak of NO detected in MgCe is not present in MgCe-Mn but a new one is observed ranging from 300–460 °C. This can be understood in conjunction with the dual-bed experiments, see Section 3.3.1, Figure 4b. Upon the addition of manganese, the low-temperature NO peak gains intensity whereas the high-temperature peak disappears. The absence of the high-temperature NO peak and the low concentration of detectable $NO_2$ in MgCe-Mn are in accordance with the dual-bed experiments and support the theory of inhibited ceria/spinel sites by manganese species.

The $NO_x$-TPD profile of MgCe-Mn-Ba is very similar to the profile obtained after adsorption in dual-bed experiments whereas the low-temperature peak associated with NO release is absent in the profile of MgCe-Ba, thus illustrating the similarity of ad-$NO_x$ species formed on $BaMnO_3$ with and without the platinum oxidation catalyst. The presence and intensity of the low-temperature NO peaks of MgCe-Mn and especially MgCe-Mn-Ba demonstrate that the corresponding ad-$NO_x$ species are only

formed if considerable amounts of $NO_2$ are available in the feed gas or in other words: if an effective NO → $NO_2$ oxidant is present.

## 4. Discussion

The effect of $MnO_x$ addition to LNT compositions based on $MgAl_2O_4/CeO_2$ on the $NO_x$ storage/release properties was investigated at an adsorption temperature of 300 °C. The results clearly show that both, compositions with and without barium, can be improved significantly by the formation of a $MnO_x$ layer on the spinel/ceria mixture. The advantages of adding manganese are different in both type of materials indicating that at least two directions in the development of novel LNT catalysts may be pursued.

1. Barium-free compositions. The formation of a manganese oxide layer on $MgAl_2O_4/CeO_2$ primarily alters the chemical nature of the generated ad-$NO_x$ species, as they exhibit lower thermostabilities than those generated without Mn-addition. This approach is clearly different from the formation of $MnO_x$-$CeO_2$ mixed oxides, which is described in several studies [45–47].

The presence of the $MnO_x$ layer significantly narrows the temperature range, in which the full amount of stored $NO_x$ is desorbed and lowers the maximum desorption temperature by about 100 °C. This finding makes the manganese modified composition an appealing candidate for the development of passive $NO_x$ adsorbers (PNA). In contrast to conventional LNT catalysts, passive $NO_x$ adsorbers are regenerated at elevated temperatures without additional rich pulses. This approach has already been described in the early 2000s [59,60] but has gained particular attention just recently due to the stricter legal requirements for $NO_x$ emissions and the implementation of the more realistic and challenging test procedure WLTP (Worldwide Harmonized Light-Duty Vehicles Test Procedure) for type approval. PNAs in combination with passive SCR catalysts can effectively improve the cold start $NO_x$ conversion at temperatures lower than 200 °C without causing additional fuel penalties [61]. The performance of PNAs is determined by (a) the ability to store $NO_x$ at low temperatures of about 150 °C and (b) effective $NO_x$ release in a narrow and low temperature range, so that the conversion over the SCR catalyst such as the recovery of $NO_x$ storages sites can take place efficiently. Ceria- and manganese-based PNAs have already been described in literature but our newly developed composition $MgAl_2O_4/CeO_2$ with $MnO_x$ appears to be an interesting and sophisticated alternative due to its narrow $NO_x$ release window from 300–450 °C [62,63]. Although the observed $NO_x$ release behaviour is very promising, the assessment of the low-temperature $NO_x$ storage efficiency has not been investigated yet and is part of ongoing studies.

2. Compositions with barium. In the case of Mn-free sample, $BaAl_2O_4$ is formed upon ageing at 850 °C, evidently leading to a decrease in $NO_x$ storage sites. The introduction of a protective layer of $MnO_x$ between spinel/ceria and barium beneficially suppresses the formation of $BaAl_2O_4$ in favour of $BaMnO_3$. This perovskite phase accommodating manganese (IV) was proven to be very active for $NO_x$ storage even at low $NO_2$/NO ratios. This beneficial effect was not observed in former investigations of Ba/Mn/alumina compositions prepared by a sequential impregnation of $\gamma$-$Al_2O_3$ with barium and manganese salts followed by calcination at only 500 °C, not leading to the formation of $BaMnO_3$ [49]. This illustrates that the temperature treatment along with the resulting phase composition has a crucial impact on the resulting $NO_x$ storage properties. The $NO_x$ retention ability and the $NO_x$ release mechanisms of the manganese modified material do not change if the sample is positioned downstream of an external Pt-catalyst. This is of enormous relevance as state of the art barium-based LNT catalysts require high levels of $NO_2$ for effective $NO_x$ conversion [54]. The observation suggests that LNT catalysts based on this formulation can tolerate a reduced noble metal (Pt/Pd) content without losing performance. Furthermore, these materials offer the opportunity for the development of new de$NO_x$ concepts, in which the LNT function is not mandatorily placed downstream of the DOC function or in which the DOC requires a certain level of $NO_x$ retention ability itself.

A detailed understanding of the chemistry involved in the generation of the various ad-$NO_x$ species presenting different thermostabilities could be gained by *operando* DRIFTS measurements

in combination with Raman spectroscopy and other sophisticated techniques. These investigations might provide a complementary overview on the diverse processes taking place on the surface of the materials during $NO_x$ storage and release. The individual contributions of the different compounds present in the compositions could be elucidated and rationalized this manner. These studies are in progress and will be presented in following publications.

## 5. Patents

WO2016/142058A1 (SASOL Germany GmbH).

**Author Contributions:** Conceptualization, M.S. and T.H.; methodology, M.S., T.H. and A.G.-G.; investigation, T.H., J.G.-M. and J.C.M.-M.; writing—original draft preparation, M.S.; writing—review and editing, A.G.-G. and J.C.M.-M.; visualization, M.S.; supervision, M.S. and A.G.-G.

**Funding:** This research received no external funding.

**Acknowledgments:** The authors thank Dirk Worch and his team (SASOL Germany GmbH) for ICP, XRD and $N_2$-physisorption measurements. A.G.-G. gratefully acknowledges the general financial support of Generalitat Valenciana (PROMETEO/2018/076), MINECO (CTQ2015-64801-R) and the UE (FEDER funding). J.C.M.-M. also acknowledges Spanish Ministry of Science, Innovation and Universities for the financial support through a FPU grant (FPU17/00603). Valuable comments provided by Karen Beckhusen, Muxin Han, Jonathan Paiz and Patrick Bussian are kindly acknowledged. The authors thank the reviewers for useful suggestions.

**Conflicts of Interest:** The authors declare no conflict of interest

## References

1. Walker, J. Johnson Matthey Sector Call—Clean Air. Available online: https://seekingalpha.com/article/4187530-johnson-matthey-jmply-sector-call-clean-air-slideshow (accessed on 2 May 2019).
2. Twigg, M.V. Catalytic control of emissions from cars. *Catal. Today* **2011**, *163*, 33–41. [CrossRef]
3. Heck, R.M.; Farrauto, R.J.; Gulati, S.T. *Catalytic Air Pollution Control*, 3rd ed.; Wiley: Hoboken, NJ, USA, 2009; pp. 158–163.
4. Metkar, P.S.; Harold, M.P.; Balakotaiah, V. Experimental and kinetic modeling study of $NH_3$-SCR of $NO_x$ on Fe-ZSM-5, Cu-chabazite and combined Fe- and Cu-zeolite monolithic catalysts. *Chem. Eng. Sci.* **2013**, *87*, 51–66. [CrossRef]
5. Koebel, M.; Madia, G.; Elsener, M. Selective catalytic reduction of NO and $NO_2$ at low temperatures. *Catal. Today* **2002**, *73*, 239–247. [CrossRef]
6. Stadlbauer, S.; Waschl, H.; Schilling, A.; del Re, L. *DOC Temperature Control for Low Temperature Operating Ranges with Post and Main Injection Actuation*; SAE International: Warrendale, PA, USA, 2013; Volume 1. [CrossRef]
7. Epling, W.S.; Campbell, L.E.; Yezerets, A.; Currier, N.W.; Parks, J.E. Overview of the Fundamental Reactions and Degradation Mechanisms of $NO_x$ Storage/Reduction Catalysts. *Catal. Rev.* **2004**, *46*, 163–245. [CrossRef]
8. Chan, D.; Gremminger, A.; Deutschmann, O. Effect of Hydrothermal Aging on Physical and Chemical Properties of a Commercial $NO_x$-Storage Catalyst. *Top. Catal.* **2013**, *56*, 293–297. [CrossRef]
9. Kubiak, L.; Castoldi, L.; Lietti, L.; Andonova, S.; Olsson, L. Mechanistic Investigation of the Reduction of $NO_x$ over Pt- and Rh-Based LNT Catalysts. *Catalysts* **2016**, *6*, 46. [CrossRef]
10. Fridell, E.; Skoglundh, M.; Westerberg, B.; Johansson, S.; Smedler, G. $NO_x$ storage in barium-containing catalysts. *J. Catal.* **1999**, *183*, 196–209. [CrossRef]
11. Lietti, L.; Forzatti, P.; Nova, I.; Tronconi, E. $NO_x$ Storage Reduction over Pt@Ba/$\gamma$-$Al_2O_3$ Catalyst. *J. Catal.* **2001**, *204*, 175–191. [CrossRef]
12. Nova, I.; Castoldi, L.; Lietti, L.; Tronconi, E.; Forzatti, P.; Prinetto, F.; Ghiotti, G. $NO_x$ adsorption study over Pt–Ba/alumina catalysts: FT-IR and pulse experiments. *J. Catal.* **2004**, *222*, 377–388. [CrossRef]
13. Kwak, J.H.; Mei, D.; Yi, C.-W.W.; Kim, D.H.; Peden, C.H.F.F.; Allard, L.F.; Szanyi, J. Understanding the nature of surface nitrates in BaO/$\gamma$-$Al_2O_3$ $NO_x$ storage materials: A combined experimental and theoretical study. *J. Catal.* **2009**, *261*, 17–22. [CrossRef]
14. Kumar, A.; Harold, M.P.; Balakotaiah, V. Isotopic studies of $NO_X$ storage and reduction on Pt/BaO/$Al_2O_3$ catalyst using temporal analysis of products. *J. Catal.* **2010**, *270*, 214–223. [CrossRef]

15. Forzatti, P.; Castoldi, L.; Nova, I.; Lietti, L.; Tronconi, E. $NO_x$ removal catalysis under lean conditions. *Catal. Today* **2006**, *117*, 316–320. [CrossRef]
16. Cumaranatunge, L.; Mulla, S.S.; Yezerets, A.; Currier, N.W.; Delgass, W.N.; Ribeiro, F.H. Ammonia is a hydrogen carrier in the regeneration of $Pt/BaO/Al_2O_3$ $NO_x$ traps with $H_2$. *J. Catal.* **2007**, *246*, 29–34. [CrossRef]
17. Bhatia, D.; Clayton, R.D.; Harold, M.P.; Balakotaiah, V. A global kinetic model for $NO_x$ storage and reduction on $Pt/BaO/Al_2O_3$ monolithic catalysts. *Catal. Today* **2009**, *147*, 250–256. [CrossRef]
18. Pereda-Ayo, B.; González-Velasco, J.R.; Burch, R.; Hardacre, C.; Chansai, S. Regeneration mechanism of a Lean $NO_x$ Trap (LNT) catalyst in the presence of NO investigated using isotope labelling techniques. *J. Catal.* **2012**, *285*, 177–186. [CrossRef]
19. Luo, J.-Y.; Epling, W.S.; Qi, G.; Li, W. Low Temperature Ceria-Based Lean $NO_x$ Traps. *Catal. Lett.* **2012**, *142*, 946–958. [CrossRef]
20. Shi, C.; Ji, Y.; Graham, U.M.; Jacobs, G.; Crocker, M.; Zhang, Z.; Wang, Y.; Toops, T.J. $NO_x$ storage and reduction properties of model ceria-based lean $NO_x$ trap catalysts. *Appl. Catal. B Environ.* **2012**, *119–120*, 183–196. [CrossRef]
21. Hilaire, S.; Wang, X.; Luo, T.; Gorte, R.J.; Wagner, J. A comparative study of water-gas-shift reaction over ceria-supported metallic catalysts. *Appl. Catal. A Gen.* **2004**, *258*, 271–276. [CrossRef]
22. Panagiotopoulou, P.; Kondarides, D.I. Effect of the nature of the support on the catalytic performance of noble metal catalysts for the water–gas shift reaction. *Catal. Today* **2006**, *112*, 49–52. [CrossRef]
23. Infantes-Molina, A.; Righini, L.; Castoldi, L.; Loricera, C.V.; Fierro, J.L.G.; Sin, A.; Lietti, L. Characterization and reactivity of Ce-promoted PtBa lean $NO_x$ trap catalysts. *Catal. Today* **2012**, *197*, 178–189. [CrossRef]
24. Say, Z.; Vovk, E.I.; Bukhtiyarov, V.I.; Ozensoy, E. Influence of ceria on the $NO_x$ reduction performance of $NO_x$ storage reduction catalysts. *Appl. Catal. B Environ.* **2013**, *142–143*, 89–100. [CrossRef]
25. Philipp, S.; Drochner, A.; Kunert, J.; Vogel, H.; Theis, J.; Lox, E.S. Investigation of NO Adsorption and $NO/O_2$ Co-adsorption on $NO_x$ -Storage-Components by DRIFT-Spectroscopy. *Top. Catal.* **2004**, *30*, 235–238. [CrossRef]
26. Ji, Y.; Toops, T.J.; Graham, U.M.; Jacobs, G.; Crocker, M. A kinetic and DRIFTS study of supported Pt catalysts for NO oxidation. *Catal. Lett.* **2006**, *110*, 29–37. [CrossRef]
27. Ryou, Y.; Lee, J.; Lee, H.; Kim, C.H.; Kim, D.H. Low temperature NO adsorption over hydrothermally aged $Pd/CeO_2$ for cold start application. *Catal. Today* **2018**, *307*, 93–101. [CrossRef]
28. Filtschew, A.; Stranz, D.; Hess, C. Mechanism of $NO_2$ storage in ceria studied using combined in situ Raman/FT-IR spectroscopy. *Phys. Chem. Chem. Phys.* **2013**, *15*, 9066–9069. [CrossRef]
29. Filtschew, A.; Hess, C. Unravelling the mechanism of NO and $NO_2$ storage in ceria: The role of defects and Ce-O surface sites. *Appl. Catal. B Environ.* **2018**, *237*, 1066–1081. [CrossRef]
30. AL-Harbi, M.; Epling, W.S. Effects of different regeneration timing protocols on the performance of a model $NO_x$ storage/reduction catalyst. *Catal. Today* **2010**, *151*, 347–353. [CrossRef]
31. Corbos, E.C.; Haneda, M.; Courtois, X.; Marecot, P.; Duprez, D.; Hamada, H. Cooperative effect of Pt–Rh/Ba/Al and CuZSM-5 catalysts for $NO_x$ reduction during periodic lean-rich atmosphere. *Catal. Commun.* **2008**, *10*, 137–141. [CrossRef]
32. Corbos, E.C.; Haneda, M.; Courtois, X.; Marecot, P.; Duprez, D.; Hamada, H. $NO_x$ abatement for lean-burn engines under lean–rich atmosphere over mixed NSR-SCR catalysts: Influences of the addition of a SCR catalyst and of the operational conditions. *Appl. Catal. A Gen.* **2009**, *365*, 187–193. [CrossRef]
33. Weibel, M.; Waldbüer, N.; Wunsch, R.; Chatterjee, D.; Bandl-Konrad, B.; Krutzsch, B. A novel approach to catalysis for $NO_x$ reduction in diesel exhaust gas. *Top. Catal.* **2009**, *52*, 1702–1708. [CrossRef]
34. Pereda-Ayo, B.; Duraiswami, D.; González-Velasco, J.R. Control of $NO_x$ storage and reduction in NSR bed for designing combined NSR–SCR systems. *Catal. Today* **2011**, *172*, 66–72. [CrossRef]
35. Castoldi, L.; Bonzi, R.; Lietti, L.; Forzatti, P.; Morandi, S.; Ghiotti, G.; Dzwigaj, S. Catalytic behaviour of hybrid LNT/SCR systems: Reactivity and in situ FTIR study. *J. Catal.* **2011**, *282*, 128–144. [CrossRef]
36. Can, F.; Courtois, X.; Royer, S.; Blanchard, G.; Rousseau, S.; Duprez, D. An overview of the production and use of ammonia in NSR+SCR coupled system for $NO_x$ reduction from lean exhaust gas. *Catal. Today* **2012**, *197*, 144–154. [CrossRef]
37. Wang, J.; Ji, Y.; Jacobs, G.; Jones, S.; Kim, D.J.; Crocker, M. Effect of aging on $NO_x$ reduction in coupled LNT–SCR systems. *Appl. Catal. B Environ.* **2014**, *148–149*, 51–61. [CrossRef]

38. Wittka, T.; Holderbaum, B.; Dittmann, P.; Pischinger, S. Experimental Investigation of Combined LNT + SCR Diesel Exhaust Aftertreatment. *Emiss. Control Sci. Technol.* **2015**, *1*, 167–182. [CrossRef]
39. Eberhardt, M.; Riedel, R.; Göbel, U.; Theis, J.; Lox, E.S. Fundamental investigations of thermal aging phenomena of model $NO_x$ storage systems. *Top. Catal.* **2004**, *30*, 135–142. [CrossRef]
40. Kim, D.H.; Chin, Y.-H.; Kwak, J.H.; Szanyi, J.; Peden, C.H.F. Changes in Ba Phases in $BaO/Al_2O_3$ upon Thermal Aging and $H_2O$ Treatment. *Catal. Lett.* **2005**, *105*, 259–268. [CrossRef]
41. Kwak, J.H.; Kim, D.H.; Szanyi, J.; Cho, S.J.; Peden, C.H.F. Enhanced High Temperature Performance of $MgAl_2O_4$-Supported Pt–BaO Lean $NO_x$ Trap Catalysts. *Top. Catal.* **2012**, *55*, 70–77. [CrossRef]
42. Jeong, S.; Youn, S.; Kim, D.H. Effect of Mg/Al ratios on the $NO_x$ storage activity over Pt-BaO/Mg–Al mixed oxides. *Catal. Today* **2014**, *231*, 155–163. [CrossRef]
43. Roy, S.; van Vegten, N.; Baiker, A. Single-step flame-made $Pt/MgAl_2O_4$—A $NO_x$ storage-reduction catalyst with unprecedented dynamic behavior and high thermal stability. *J. Catal.* **2010**, *271*, 125–131. [CrossRef]
44. Casapu, M.; Grunwaldt, J.-D.; Maciejewski, M.; Wittrock, M.; Göbel, U.; Baiker, A. Formation and stability of barium aluminate and cerate in $NO_x$ storage-reduction catalysts. *Appl. Catal. B Environ.* **2006**, *63*, 232–242. [CrossRef]
45. Wu, X.; Lin, F.; Xu, H.; Weng, D. Effects of adsorbed and gaseous $NO_x$ species on catalytic oxidation of diesel soot with $MnO_x$-$CeO_2$ mixed oxides. *Appl. Catal. B Environ.* **2010**, *96*, 101–109. [CrossRef]
46. Shen, Q.; Zhang, L.; Sun, N.; Wang, H.; Zhong, L.; He, C.; Wei, W.; Sun, Y. Hollow $MnO_x$-$CeO_2$ mixed oxides as highly efficient catalysts in NO oxidation. *Chem. Eng. J.* **2017**, *322*, 46–55. [CrossRef]
47. Qi, G.; Li, W. NO oxidation to $NO_2$ over manganese-cerium mixed oxides. *Catal. Today* **2015**, *258*, 205–213. [CrossRef]
48. Le Phuc, N.; Courtois, X.; Can, F.; Royer, S.; Marecot, P.; Duprez, D. $NO_x$ removal efficiency and ammonia selectivity during the $NO_x$ storage-reduction process over $Pt/BaO(Fe, Mn, Ce)/Al_2O_3$ model catalysts. Part II: Influence of Ce and Mn–Ce addition. *Appl. Catal. B Environ.* **2011**, *102*, 353–361. [CrossRef]
49. Le-Phuc, N. Removal of $NO_x$ in the presence of oxygen over $Mn/BaO/Al_2O_3$ catalysts. *Mater. Sci. Nanaotechnol.* **2017**, *1*, 37–40.
50. Zhang, Z.; Chen, B.; Wang, X.; Xu, L.; Au, C.; Shi, C.; Crocker, M. $NO_x$ storage and reduction properties of model manganese-based lean $NO_x$ trap catalysts. *Appl. Catal. B Environ.* **2015**, *165*, 232–244. [CrossRef]
51. Xiao, J.; Li, X.; Deng, S.; Wang, F.; Wang, L. $NO_x$ storage-reduction over combined catalyst $Mn/Ba/Al_2O_3$–$Pt/Ba/Al_2O_3$. *Catal. Commun.* **2008**, *9*, 563–567. [CrossRef]
52. Schöneborn, M.; Harmening, T.; Niemeyer, D.; Rolfs, S.; Fabian, J. $NO_x$ Trap Catalyst Support Material with Improved Stability against $BaAl_2O_4$ Formation. Patent No. WO2016142058A1, 15 September 2016.
53. Adouane, D.; Dutilleul, H.; Guibert, P.; Darcy, P.; Costa, P. Da Effect of thermal ageing on structure and reactivity of commercial Lean $NO_x$ trap: From laboratory to engine scale. In Proceedings of the 7th International Conference on Environmental Catalysis, Lyon, France, 2–6 September 2012.
54. Al-Harbi, M.; Epling, W.S. Investigating the effect of NO versus $NO_2$ on the performance of a model $NO_x$ storage/reduction catalyst. *Catal. Lett.* **2009**, *130*, 121–129. [CrossRef]
55. Gao, Y.; Wu, X.; Liu, S.; Weng, D.; Zhang, H.; Ran, R. Formation of $BaMnO_3$ in $Ba/MnO_x$-$CeO_2$ catalyst upon the hydrothermal ageing and its effects on oxide sintering and soot oxidation activity. *Catal. Today* **2015**, *253*, 83–88. [CrossRef]
56. Xiao, J.H.; Li, X.H.; Deng, S.; Xu, J.C.; Wang, L.F. The $NO_x$ oxidation-storage and tolerance of $SO_2$ poison of $Mn/Ba/Al_2O_3$ catalyst. *Acta Phys.-Chim. Sin.* **2006**, *22*, 815–819. [CrossRef]
57. Kapteijn, F.; Vanlangeveld, A.D.; Moulijn, J.A.; Andreini, A.; Vuurman, M.A.; Turek, A.M.; Jehng, J.M.; Wachs, I.E. Alumina-Supported Manganese Oxide Catalysts: I. Characterization: Effect of Precursor and Loading. *J. Catal.* **1994**, *150*, 94–104. [CrossRef]
58. Guo, L.H.; Guo, L.; Zhao, D.Y.; Gao, Z.N.; Tian, Y.; Ding, T.; Zhang, J.; Zheng, L.R.; Li, X.G. Oxidizing, trapping and releasing $NO_x$ over model manganese oxides in alternative lean-burn/fuel-rich atmospheres at low temperatures. *Catal. Today* **2017**, *297*, 27–35. [CrossRef]
59. Feeley, J.S.; Farrauto, R.J.; Deeba, M. Method and Apparatus for NOx Abatement in Lean Gaseous Streams. U.S. Patent No. 6471924B1, 29 October 2002.
60. Jarvis, M.; Adams, K.M. Method for Converting Exhaust Gases from a Diesel Engine using Nitrogen Oxide Absorbent. U.S. Patent No. 6182443B1, 6 February 2001.

61. Gu, Y.; Epling, W.S. Passive $NO_x$ adsorber: An overview of catalyst performance and reaction chemistry. *Appl. Catal. A Gen.* **2019**, *570*, 1–14. [CrossRef]
62. Jones, S.; Ji, Y.; Bueno-Lopez, A.; Song, Y.; Crocker, M. $CeO_2$-$M_2O_3$ Passive $NO_x$ Adsorbers for Cold Start Applications. *Emiss. Control Sci. Technol.* **2017**, *3*, 59–72. [CrossRef]
63. Ji, Y.; Xu, D.; Crocker, M.; Theis, J.R.; Lambert, C.; Bueno-Lopez, A.; Harris, D.; Scapens, D. Mn-based mixed oxides for low temperature $NO_x$ adsorber applications. *Appl. Catal. A Gen.* **2018**, *567*, 90–101. [CrossRef]